Submitted to

International Europhysics Conference on High Energy Physics, EPS03, July 17-23, 2003, Aachen
(Abstract **082** Parallel Session **4**)

XXI International Symposium on Lepton and Photon Interactions, LP03, August 11-16, 2003, Fermilab

www-h1.desy.de/h1/www/publications/conf/conf_list.html

Measurement of the Inclusive Deep Inelastic Scattering Cross Section at $Q^2 \sim 1$ GeV^2 with the H1 Experiment

H1 Collaboration

Abstract

New data are presented of the inclusive ep scattering cross section in the kinematic region of very low Bjorken x and four-momentum transfer squared $Q^2 \sim 1$ GeV^2, in the transition region from the non-perturbative to the deep-inelastic domain. The data were taken at HERA in the summer 2000, with a proton beam energy of 920 GeV and an electron beam energy of 27.5 GeV. In a dedicated HERA run, the interaction vertex was shifted by +70 cm, thereby accessing a region of lower Q^2 than at nominal vertex position. With a fourfold increase in statistics and new instrumentation the accuracy of the measurement is improved as compared to previous shifted vertex data. The cross-section measurement is used to obtain new, preliminary data on the proton structure function $F_2(x, Q^2)$, and its rise towards low x is studied.

1 Introduction

The region of momentum transfer squared Q^2 around 1 GeV^2 deserves particular attention because it corresponds to the transition between the non-perturbative and the perturbative domains in deep-inelastic scattering (DIS). Thus at HERA a special positron-proton scattering run was performed in which the interaction vertex was shifted by about 70 cm in the proton beam direction which allows larger positron scattering angles[1] $\theta_e = \angle(\vec{e}\,', \vec{p})$ and thus lower values of Q^2 to be accessed.

The data presented here were taken in August 2000. With a luminosity of 0.6 pb^{-1} the statistics is larger by about a factor of four as compared to the initial shifted vertex run in 1995 which lead to first data on the proton structure function $F_2(x, Q^2)$ in this kinematic region, by H1 [1] and ZEUS [2]. Based on the larger statistics and using the new Backward Silicon Tracker (BST), the accuracy of the previous first shifted vertex data of H1 is superseded by this analysis.

Besides extending the kinematic range to lower Q^2 the new shifted vertex data also overlaps, for larger Q^2, with nominal vertex data presented recently [3]. These new low Q^2 data sets use an extended silicon tracker and were obtained with a proton beam energy, E_p, enlarged from 820 GeV to 920 GeV. They thus complement the published H1 measurement [4] of the inclusive neutral current deep-inelastic scattering (DIS) cross section, $\sigma(ep \to eX)$. The kinematic plane and its extension with the new data towards low Q^2 is illustrated in Figure 1.

The inclusive measurements determine the cross section which at low Q^2 in the one-photon exchange approximation can be written in reduced form as

$$\frac{Q^4 x}{2\pi\alpha^2 Y_+} \cdot \frac{d^2\sigma}{dx dQ^2} = \sigma_r = F_2(x, Q^2) - \frac{y^2}{Y_+} \cdot F_L(x, Q^2). \tag{1}$$

Here y is the inelasticity which is related to x and Q^2 as $y = Q^2/sx$. The beam energies determine the centre of mass energy squared, $s = 4E_e E_p$, and Y_+ is defined as $1 + (1-y)^2$. In the region of inelasticity below $y = 0.6$ the contribution of the longitudinal structure function $F_L(x, Q^2)$ is small due to the kinematic factor y^2/Y_+ and since $F_L \leq F_2$. Thus the measurement of σ_r at lower y directly determines F_2 with a small correction for F_L.

Section 2 of this paper describes the experimental methods, i.e. the kinematic reconstruction with the H1 detector, the event selection, simulation and calibration. The cross-section measurement and the extraction of the structure function $F_2(x, Q^2)$ are discussed in Section 3 which is complemented by a study of the rise of $F_2(x, Q^2)$ towards low x. A brief summary is given in Section 4.

2 Experimental Methods

2.1 Kinematic Reconstruction with the H1 Detector

The event kinematics are reconstructed using the energy E'_e and the polar angle θ_e of the scattered positron according to the relations

$$y_e = 1 - \frac{E'_e}{E_e}\,\sin^2(\theta_e/2); \qquad Q^2_e = \frac{E'^2_e \sin^2\theta_e}{1-y_e}. \tag{2}$$

[1] Note that the polar angles θ are defined with respect to the proton beam direction.

which define the electron reconstruction method. The scattered positron energy E'_e is measured in the backward electromagnetic lead scintillating fibre calorimeter SPACAL [5]. The polar angle θ_e is measured in the BST [6, 7].

Since the resolution of y_e degrades as $1/y$, the kinematics at low y are obtained using information from the hadronic final state which is reconstructed in the Liquid Argon calorimeter (LAr) and the SPACAL [8]. This determines the inelasticity variable y to be

$$y_h = \frac{\sum_i (E_i - p_{z,i})}{2E_e} = \frac{\sum_h}{2E_e}, \tag{3}$$

where E_i and $p_{z,i}$ are the energy and longitudinal momentum component of a final state particle i, the masses being neglected. In the analysis Q^2 and y are also determined using the Σ method which combines E'_e, θ_e, and y_h according to

$$y_\Sigma = \frac{y_h}{1 + y_h - y_e} = \frac{\sum_h}{\sum_h + E'_e(1 - cos\theta_e)}; \qquad Q^2_\Sigma = \frac{E'^2_e \sin^2\theta_e}{1 - y_\Sigma}. \tag{4}$$

The kinematics are reconstructed using both the electron method and the sigma method which allows the final cross section to be obtained with optimum accuracy. For the cross section determination the electron method is used at $y > 0.05$. At $y < 0.05$, where the resolution of y_e degrades, the kinematics are reconstructed with the Σ method.

The hadronic scattering angle is defined as

$$\tan\frac{\theta_h}{2} = \frac{\sum_h}{P_{t,h}}, \tag{5}$$

where $P_{t,h}$ is the total transverse momentum of the hadronic final state particles. The two angles θ_e and θ_h are used to calibrate the positron energy measurement of the SPACAL calorimeter.

2.2 Triggers and Event Selection

The data are triggered using the local energy sums in the SPACAL calorimeter with an energy threshold set to 6 GeV. Low energy deposits can also be caused by hadrons and photons from events at very low $Q^2 \ll 1$ GeV^2 which mimic a positron signal in the SPACAL. Part of these photoproduction background events is recognised by tagging a scattered positron at very small angles in the electron tagger calorimeter upstream the positron beam.

The efficiency of all trigger elements exceeds 98% and is controlled by independent tracking triggers to an accuracy of 0.5%. From a monitor event sample, defined by a vertex accurately reconstructed in the central tracker and by a high energy SPACAL cluster, the BST efficiency is determined and the Monte-Carlo simulation correspondingly adjusted. The hit efficiency of the BST is 97% on average, excluding a few malfunctioning sensor modules.

DIS events are required to have a vertex reconstructed from a track measured in the BST and its intersection with the beam axis. The track has to be associated to the highest energetic cluster in the SPACAL, where the cluster is required to extend by less than two Molière radii in the transverse plane. Any energy behind the electromagnetic cluster measured in the

z vertex position	$\|z - 70\| < 45$cm
SPACAL cluster radius	< 4cm
SPACAL-BST matching	$\delta r < 2$cm
electromagnetic SPACAL energy	> 7 GeV
hadronic SPACAL energy	$< 15\%$ of E'_e
total $E - p_z$	> 35 GeV

Table 1: *Basic criteria to select DIS events.*

hadronic SPACAL may not exceed a small fraction of E'. QED radiative effects and background contributions are suppressed requiring energy-momentum conservation using the total $E - p_z$ reconstructed in the detector. The criteria of the DIS event selection are summarised in Table 1.

A high statistics simulation of DIS events is performed using the program DJANGO [9] with a parameterisation of the parton distributions (MRST 3,75) [10] extended to very low Q^2. For the extraction of the cross section and comparisons of experimental with simulated spectra, a recent fit to previous low Q^2 data [4, 11] was used for reweighting which is based on the fractal proton structure concept. This fit [12] describes the data in the non-perturbative region and the data in the deep-inelastic domain very well. Photoproduction events are simulated with the program PHOJET [13]. The simulated events are subject to the same reconstruction and analysis chain as the real data. In the comparisons of experimental distributions with the Monte-Carlo spectra, these are normalised to the measured luminosity.

The luminosity as determined from the cross section of the elastic bremsstrahlung process is measured with a precision of 1.8% .

2.3 Alignment and Calibration

The measurement of the polar angle θ_e requires the Backward Silicon Tracker to be accurately aligned. After the internal adjustment of the detector planes, the BST is aligned by comparing the interaction vertex (z_v) reconstructed from the electron in the BST with that reconstructed from hadrons in the central tracker (z). A measurement accuracy of θ_e of 0.3 mrad is obtained as deduced from comparison of the angle measured in the BST with the one resulting from z_v and the hit position in the Backward Drift Chamber (BDC) in front of the SPACAL. The SPACAL and the BDC positions are adjusted using QED Compton events which have the signature of back-to-back positron and photon clusters in the plane transverse to the beam axis.

The energy scale of the electromagnetic SPACAL cells is determined using the double angle method [14] in the region of large $E' > 20$ GeV to within a remaining uncertainty of 0.3%. This scale was verified in the low energy range, at about 7 GeV, to better than 2% from a comparison of E' with the corresponding momentum p, measured with the BST, and the transverse vertex position [3]. The hadronic energy scales in the LAr calorimeter and in the SPACAL are determined to an accuracy of 2% and 5%, respectively, using a global minimisation technique [6] for the influence of the calorimeter constants on the transverse momentum balance for the DIS events. A direct verification of the electromagnetic and the hadronic energy scale uncertainties is obtained from an extension of the cross-section measurement, using the electron method down to very low $y \geq 0.005$ and the sigma method up to large $y \leq 0.7$, respectively. The resulting cross sections agree to within the statistical accuracy.

2.4 Systematic Uncertainties

A precise measurement of the DIS cross section requires the data to be corrected for acceptance, inefficiency, resolution and radiative effects. It is thus important to compare experimental and simulated distributions. Such control distributions are shown in Figure 2. The experimental distributions for geometric quantities, $(z_v,\ \theta_e)$, energy (E'_e) and basic kinematic variables $(x_e,\ Q^2_e,\ y_\Sigma)$, are seen to be well described by the DIS simulation. The track requirement with the BST and the momentum conservation requirement ($E - p_z$ cut) reduce the photoproduction background in this analysis to a very small level. Note that the normalisation of the photoproduction simulation was adjusted by about 20% based on the electron tagger information. The full size of this renormalisation factor is chosen as the uncertainty of the photoproduction simulation luminosity.

The uncertainties of this cross-section measurement are divided into four different kinds:

- The data have a normalisation uncertainty of 1.8% resulting from the uncertainty of the luminosity measurement. This uncertainty is not included in any error bar subsequently shown.
- The statistical uncertainty of the data is about 1-5%.
- An about 2% uncorrelated cross section uncertainty is due to the simulated event statistics. Moreover, uncorrelated errors with weak kinematic dependencies result from the BST track reconstruction (1-2%), from the uncertainty of the radiative corrections (1%) and from the determination of the SPACAL trigger efficiency (0.5%).
- Correlated cross section uncertainties are due to the E' and E_h measurements (0.5-2%), the θ_e reconstruction (1%), the calorimeter noise (about 2-5% at low y) and due to the photoproduction background (2% at large y).

The total cross section uncertainty is about 4% in the bulk data region. This is an approximately twofold increase in measurement accuracy as compared to the previous H1 shifted vertex data [1]. Moreover, since the vertex is not anymore reconstructed from hadrons but from the positron track in the BST, the new data extend by one order of magnitude deeper into the low y region than the 1995 data. Thus they close the kinematic gap to the fixed target μp data from NMC.

3 Results

3.1 Cross Section and the Proton Structure Function F_2

The kinematic region accessed in this measurement is divided into nine Q^2 intervals in the range $0.3 < Q^2 < 4.2$ GeV^2. The data are also divided in bins of y. The binning is adapted to the resolution in the measurement of the kinematic variables. Bins are accepted if the purity and stability are bigger than 30%. Here the purity (stability) is defined as the number of simulated events which originate from a bin and which are reconstructed in it, divided by the number of reconstructed (generated) events in that bin.

The measured reduced cross-section, shown in Figure 3, represents the most accurate low x inclusive DIS data in the transition region, $Q^2 \sim 1$ GeV^2, obtained so far[2]. It is seen that the shifted vertex data agree well with the recently presented H1 1999 nominal vertex data in the region of overlap, extending the measurement to lower Q^2. The new data are found to be consistent also with data at larger Bjorken x, from the ZEUS measurement with the Beam Pipe Tracker (BPT) [11], placed downstream the positron beam direction, and from the NMC Collaboration [15].

The present cross-section data cover a region of inelasticity up to $y = 0.75$. At large y effects of the longitudinal structure function may be observed leading to a taming of the cross section rise towards low x. Such a behaviour is indeed observed in the data, see Figure 3. The solid curves in Figure 3 represent a calculation of the reduced cross section using the fractal model [12] for F_2 and a dipole model calculation of F_L [16]. In this dipole model $F_L(x, Q^2)$, for $x = 10^{-4}$, rises from about 0.05 up to 0.2 in the range $Q^2 = 0.35...3.5$ GeV^2 covered by the data. Using this prediction for F_L, new data are obtained on the proton structure function $F_2(x, Q^2)$ in the range $0.003 < y < 0.6$, which are shown in Figure 4. The data are in very good agreement both with the recently published H1 data and also with the preliminary data from a dedicated run at the end of 1999 [3] which used the same BST-SPACAL detector configuration and analysis methods.

In Figure 4 the new F_2 data are compared with phenomenological predictions obtained from fits to previous data. The best description is given by the fractal model parameterisation [12] (solid curves) the few parameters of which were determined with the ZEUS BPT data [11] and the published low Q^2 H1 data [4]. The ALLM97 [17] parameterisation (dashed-dotted curves) similarly used previous data which leads to an acceptable description of the present F_2 data with a slightly stronger rise towards x for $Q^2 \geq 1$ GeV^2 than is observed in the H1 data. Also shown is the F_2 representation from the H1 NLO QCD fit [4] (dashed curves). The fit included only data with $Q^2 \geq 3.5$ GeV^2. Its backward extrapolation is here seen to undershoot the measured behaviour for lower Q^2. At $Q^2 \lesssim 1$ GeV^2 the strong coupling constant $\alpha_s(Q^2)$ is too large which renders a NLO QCD comparison with data meaningless.

Another representation of this data (see Figure 5) shows the virtual photon-proton cross section, $\sigma_{\gamma^* p} \propto F_2/Q^2$, as a function of Q^2 at fixed $W^2 \simeq sy$, where W is the invariant mass of the $\gamma^* p$ system. The new data fill the gap between previous data obtained at lower and higher Q^2 and reach similar accuracy. As for the previous figure the three different parametrisations of F_2 are presented. At $Q^2 \simeq 1$ GeV^2 the ALLM97 parameterisation is too large at high W and the QCD fit fails. The fractal model fit, for $Q^2 \rightarrow 0$, is too steep to describe the total photoproduction cross-section data (not shown here), which, however, can be cured by considering mass effects in the fractal ansatz [18].

[2] The larger x H1 data at $Q^2 \leq 1$ GeV^2 are measured using the lower edge of the SPACAL calorimeter and of the Silicon tracker (BST) which causes larger statistical and systematic uncertainties.

3.2 Rise of $F_2(x, Q^2)$ Towards Low x

Recently the H1 Collaboration has presented [19] a measurement of the derivative

$$\left(\frac{\partial \ln F_2(x,Q^2)}{\partial \ln x}\right)_{Q^2} \equiv -\lambda(x,Q^2) \tag{6}$$

which quantifies the behaviour of the rise of $F_2(x, Q^2)$ towards low x at fixed Q^2. With the present data this measurement can be extended to lower Q^2, as is demonstrated in Figure 6. In the region of overlap the new measurement confirms the previous data. The trend of the derivative to be independent of x at fixed Q^2 is seen to hold down to about 1 GeV^2, the accuracy and kinematic range of the data below this value, however, prevent definite conclusions.

The independence of the derivative $\lambda(x, Q^2)$ of x implies that the x dependence of F_2 at low x is consistent with a power law, $F_2 \propto x^{-\lambda}$, for fixed Q^2, and that the rise of F_2, i.e. $(\partial F_2/\partial x)_{Q^2}$, is proportional to F_2/x. As for the previously published H1 data, the exponent $\lambda(Q^2)$ was determined from fits of the form $F_2(x, Q^2) = c(Q^2) \cdot x^{-\lambda(Q^2)}$. The result is shown in Figure 7. Within the accuracy reached, the trend of a linear decrease of $\lambda(Q^2)$ is found to continue down to $Q^2 \sim 1$ GeV^2 with a slight tendency, at very low Q^2, to lie above.

In order to increase the x range of this investigation the new data are combined with published H1 data [4], with NMC data [15] and with ZEUS data [11] at very low Q^2 (see Figure 8). The decrease of $\lambda(Q^2)$ towards low Q^2 is now seen to deviate significantly from an extrapolation of the linear behaviour determined from the data in the deep inelastic scattering region [19]. Correlated with this behaviour, the function $c(Q^2)$ is observed to decrease with decreasing Q^2, for $Q^2 < 3.5$ GeV^2.

4 Summary

A new measurement of the deep-inelastic positron-proton scattering cross section is presented for squared four-momentum transfers $0.35 \leq Q^2 \leq 3.5\,\mathrm{GeV}^2$ and for Bjorken-x values $7 \cdot 10^{-6} \leq x \leq 2 \cdot 10^{-3}$. The data were taken in August 2000 with the interaction-vertex shifted by 70 cm in proton-beam direction thereby allowing the acceptance to be extended to lower Q^2 than previously accessible. The scattered positron angle and the interaction vertex are reconstructed using the extended Backward Silicon Tracker of the H1 experiment. The hadronic final state is reconstructed using the LAr and SPACAL calorimeters. Thus the measurement range in inelasticity y is much extended and the measurement uncertainty halved as compared to previous H1 shifted vertex data.

This measurement provides the first precise low x data on the inclusive DIS cross-section in the transition region from the non-perturbative to the deep-inelastic domain. A taming of the cross section rise towards low x is observed which occurs at large inelasticities $y \simeq 0.5$ and thus is attributed to a non-vanishing longitudinal structure function F_L at low Q^2. In the kinematic region of this measurement $F_2(x, Q^2)$ still rises towards low x at fixed Q^2 like $F_2(x, Q^2) = c(Q^2) \cdot x^{-\lambda(Q^2)}$. The functions $c(Q^2)$ and $\lambda(Q^2)$, however, are observed to deviate from expectations based on the linear dependence of c and λ on $\ln Q^2$ as determined in the deep inelastic scattering region.

Acknowledgements We are very grateful to the HERA machine group whose outstanding efforts made this experiment possible. We acknowledge the support of the DESY technical staff. We appreciate the substantial effort of the engineers and technicians who constructed and maintain the detector. We thank the funding agencies for financial support of this experiment. We wish to thank the DESY directorate for the support and hospitality extended to the non-DESY members of the collaboration.

References

[1] H1 Collaboration, C. Adloff *et al.*, Nucl. Phys. **B497** (1997) 3.

[2] ZEUS Collaboration, J. Breitweg *et al.*, Eur. Phys. J. C **7** (1999) 609-630, [hep-ex/9809005].

[3] D. Eckstein [H1 Collaboration], in“DIS 2001 - 9th Int. Workshop on Deep Inelastic Scattering”, G. Bruni, G. Iacobucci and R. Nania (eds.), World Scientific (2002);
H1 Collaboration, paper 79 subm. to Int. Europhysics Conference on High Energy Physics EPS-HEP 2001, Budapest.

[4] H1 Collaboration, C. Adloff *et al.*, Eur. Phys. J. C **21** (2001) 33-61, [hep-ex/0012153].

[5] R. Appuhn *et al.*, Nucl. Instr. and Meth. **A386** (1996) 397.

[6] V.V. Arkadov, PhD Thesis, Berlin, Humboldt-University, 2000, DESY-Thesis-2000-046.

[7] D. Eckstein, PhD Thesis, Berlin, Humboldt-University, 2002, DESY-Thesis-2002-008.

[8] H1 Collaboration, I. Abt *et al.*, Nucl. Instr. and Meth. **A386** (1997) 310 and **A386** (1997) 348.

[9] G. A. Schuler and H. Spiesberger, Proc. Workshop on HERA Physics, Vol 3, eds. W. Buchmüller and G. Ingelman, Hamburg, DESY (1992), p. 1419;
A. Kwiatkowski, H. Spiesberger and H.-J. Möhring, Comp. Phys. Comm. **69** (1992) 155;
L. Lönnblad, Comp. Phys. Comm. **71** (1992) 15.

[10] PDFLIB: The Parton Density Functions Library, Version 8.04, MRST set 75, CERN.

[11] ZEUS Collaboration, J. Breitweg *et al.*, Phys. Lett. B **487** (2000) 53.

[12] T. Laštovička, Self-similar Properties of the Proton Structure at low x, Eur. Phys. J. C, to appear, [hep-ph/0203260] (2002).

[13] R. Engel and J. Ranft, Phys. Rev. **D54** (1996) 4244.

[14] A.A. Glazov, PhD Thesis, Berlin, Humboldt-University, 1998.

[15] NMC Collaboration, M. Arneodo *et al.*, Nucl. Phys. **B483** (1997) 3.

[16] K. Golec-Biernat and M. Wüsthoff, Phys. Rev. D **59** (1999) 014017, [hep-ph/9807513].

[17] H. Abramowicz and A. Levy, The ALLM parameterization of sigma(tot)(gamma* p): An update, DESY-97-251, [hep-ph/9712415] (1997).

[18] T. Laštovička, in "DIS 2002 - 10th Int. Workshop on Deep Inelastic Scattering", to appear in Acta Phys. Polonica B.

[19] H1 Collaboration, C. Adloff *et al.*, Phys. Lett. B **520** (2001) 183, [hep-ex/0108035].

[20] BCDMS Collaboration, A. C. Benvenuti *et al.*, Phys. Lett. B **223** (1989) 485, CERN preprint CERN-EP/89-06.

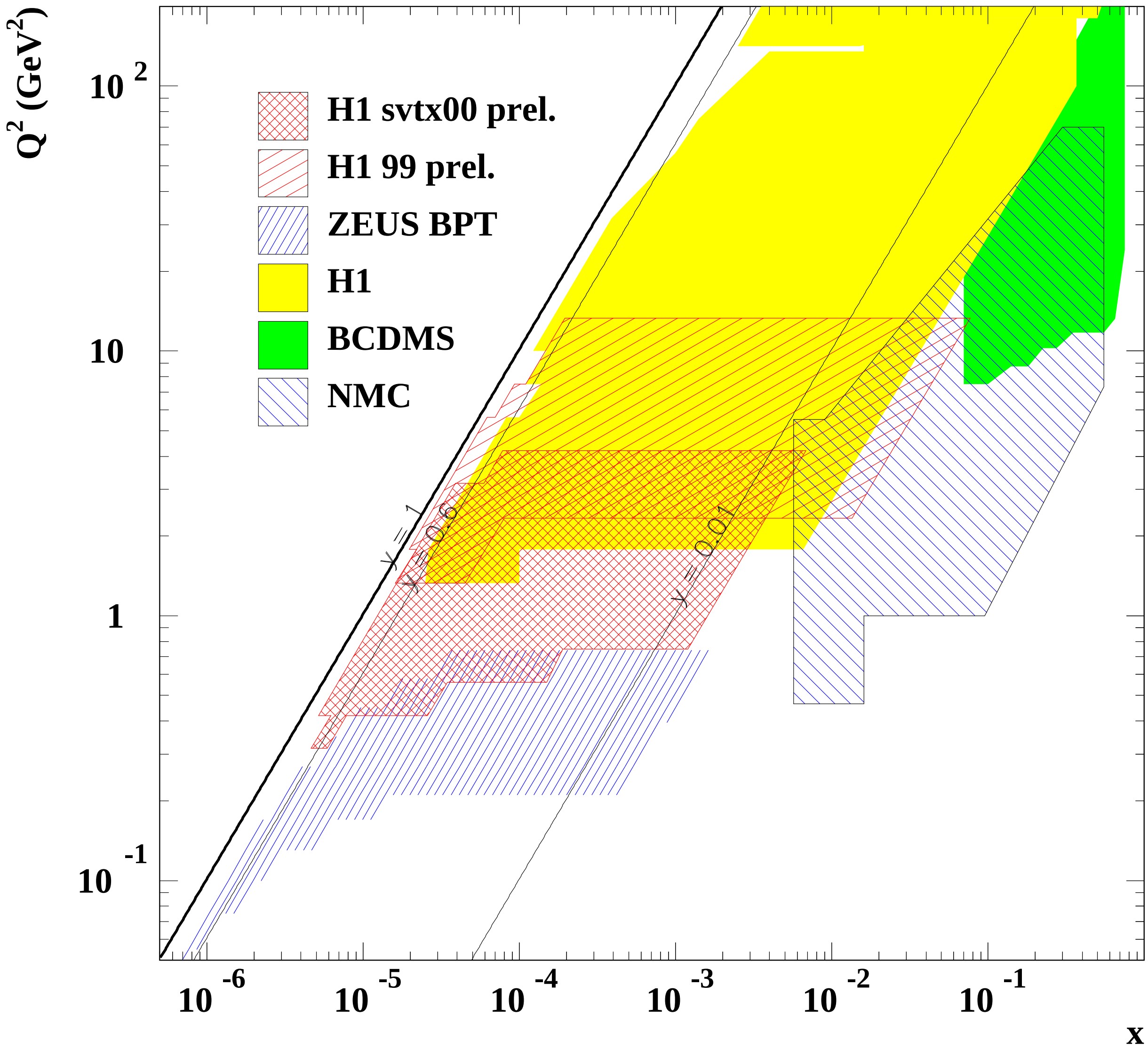

Figure 1: Kinematic region covered by the preliminary H1 measurements at 920 GeV proton beam energy [3] (H1 svtx00 prel. and H1 99 prel.), by the recently published H1 data at 820 GeV [4], by the ZEUS Backward Pipe Detector (BPT) [11] and by the muon-proton scattering experiments NMC [15] and BCDMS [20]. The lines of constant y correspond to this analysis, i.e. $E_e = 27.5$ GeV and $E_p = 920$ GeV.

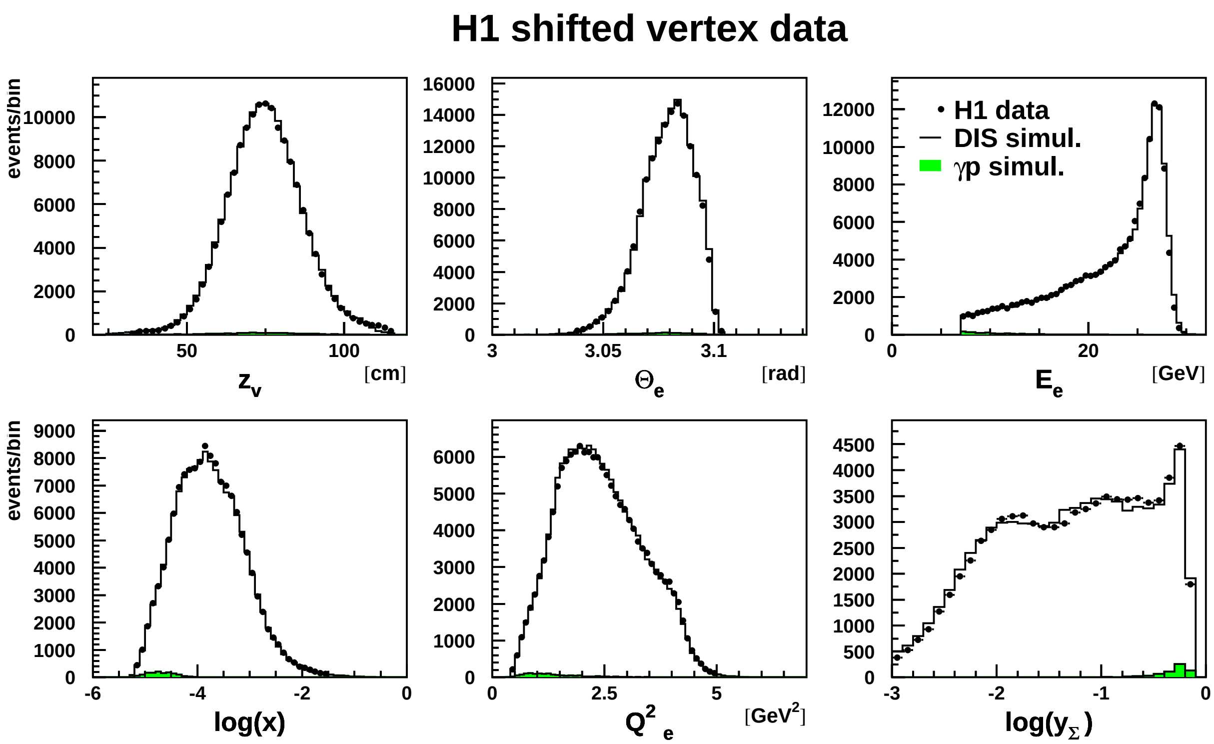

Figure 2: Event distributions of: z vertex position and polar angle reconstructed with the BST; energy of the scattered positron candidate measured in the SPACAL backward calorimeter; Bjorken-x and Q^2 from the positron kinematics and inelasticity from the Σ method, see text. Histograms: DIS and photoproduction background (green shaded) simulation normalised to the measured luminosity.

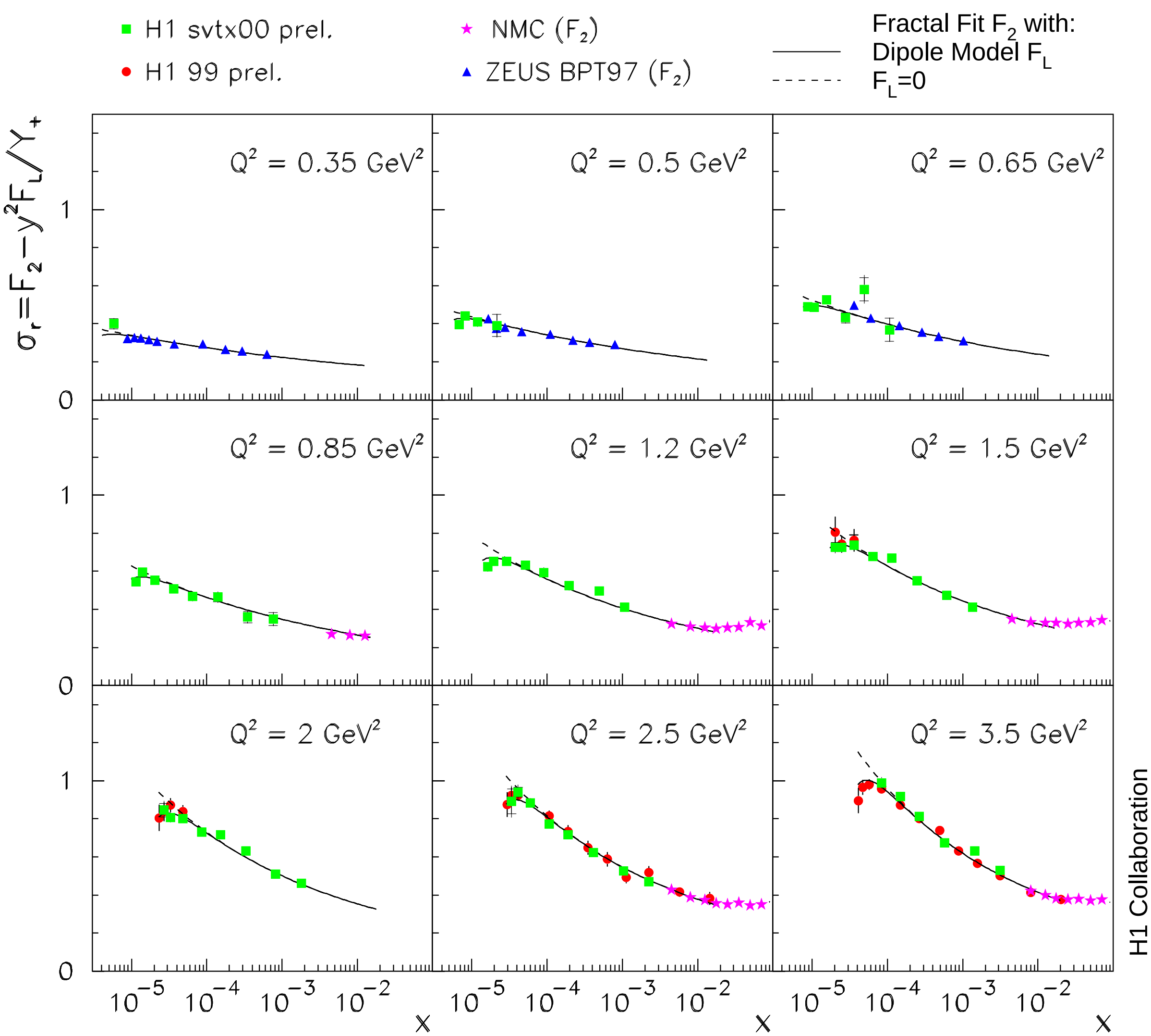

Figure 3: Measurements of the inclusive DIS cross section - H1 shifted vertex data 2000, this analysis (green squares), and H199 nominal vertex data (red points), compared to larger x data from ZEUS (BPT97 blue triangles) and from NMC (purple stars). The curves are a phenomenological parameterisation of the cross section calculating F_2 within the fractal proton structure concept and using a dipole model prediction for F_L (solid) and $F_L = 0$ (dashed).

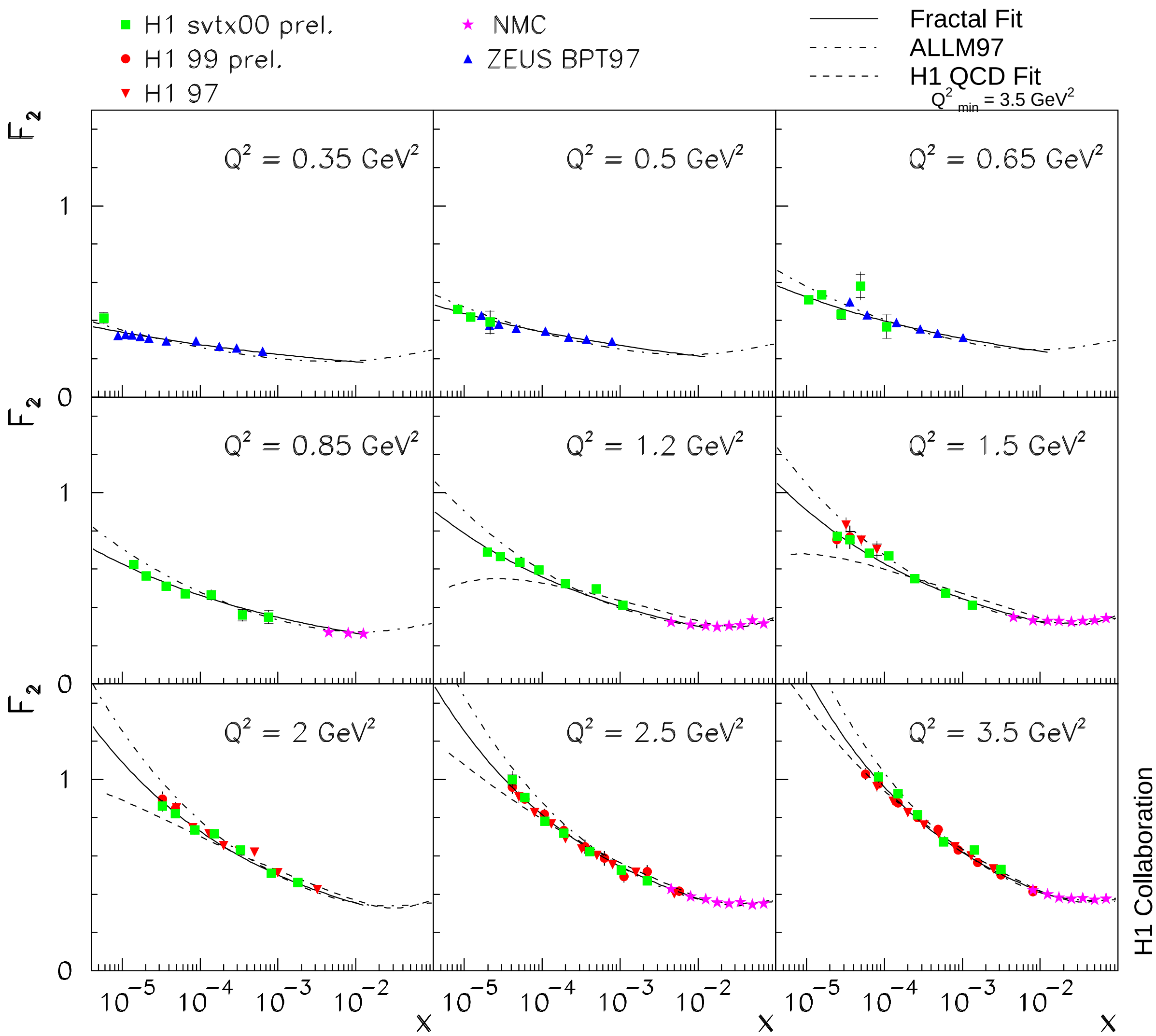

Figure 4: Measurements of the structure function $F_2(x,Q^2)$ - H1 shifted vertex data 2000, this analysis (green squares), H1 99 and 97 nominal vertex data (red points and triangles), compared to larger x data from ZEUS (BPT97 blue triangles) and from NMC (purple stars). Solid curves: phenomenological parameterisation of $F_2(x,Q^2)$ based on the fractal proton structure concept; Dashed curves: NLO QCD fit to the H1 96/97 data which was performed to data for $Q^2 \geq 3.5$ GeV^2, i.e. it is extrapolated here into the lower Q^2 region. Dashed-dotted curves: ALLM97.

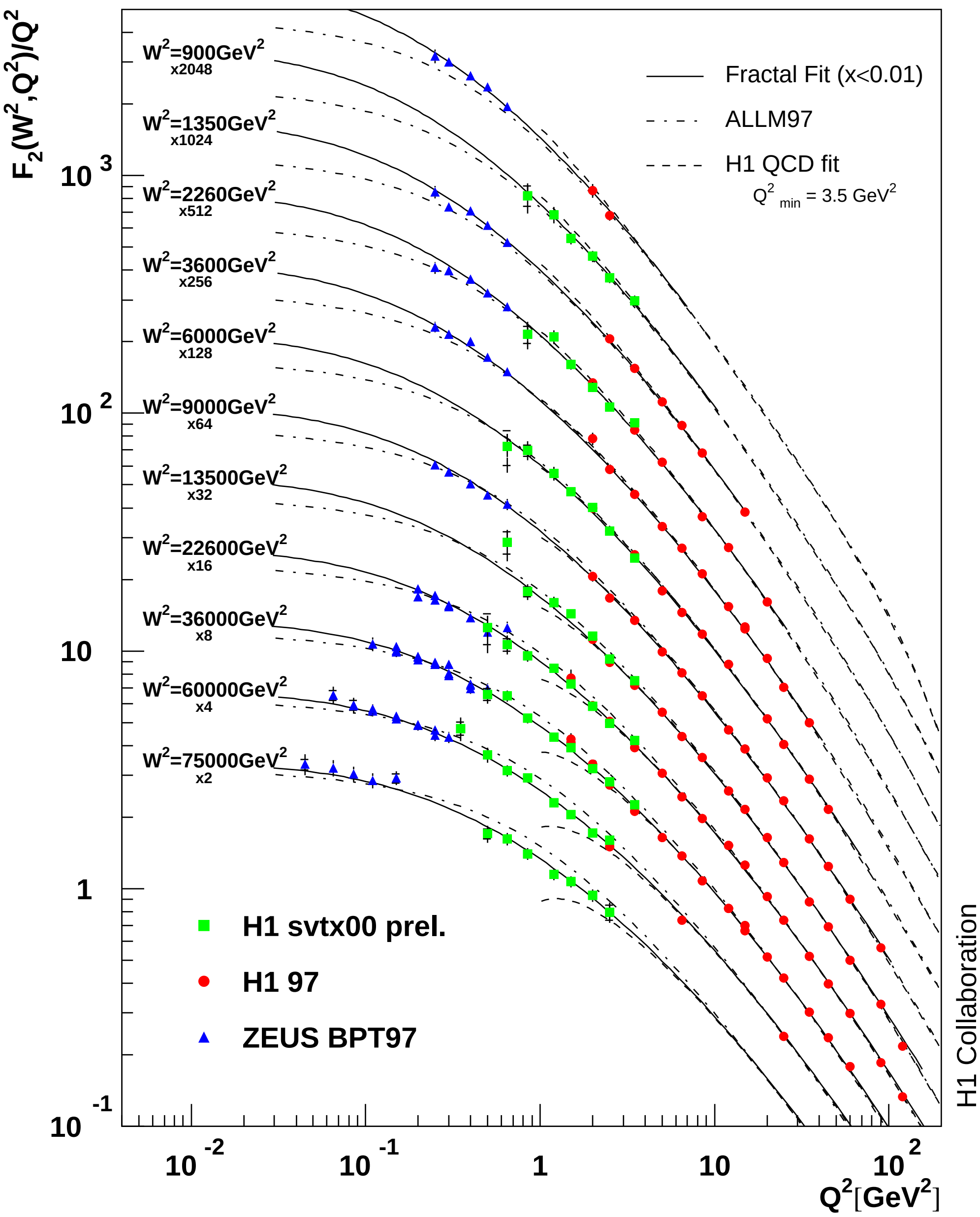

Figure 5: Measurements of the structure function F_2 represented as F_2/Q^2 which is proportional to the total cross section for virtual photon-proton scattering. Green squares: H1 2000 shifted vertex data, this analysis. The solid curves represent the fractal F_2 fit which was fixed using the two data sets shown at lower Q^2 (ZEUS 97 BPT, blue triangles) and higher Q^2 (H1 96/97, red points). Dashed-dotted curves: the ALLM97 parameterisation; Dashed curves: H1 NLO QCD fit, with $Q^2_{min} = 3.5$ GeV^2, extrapolated down to 1 GeV^2.

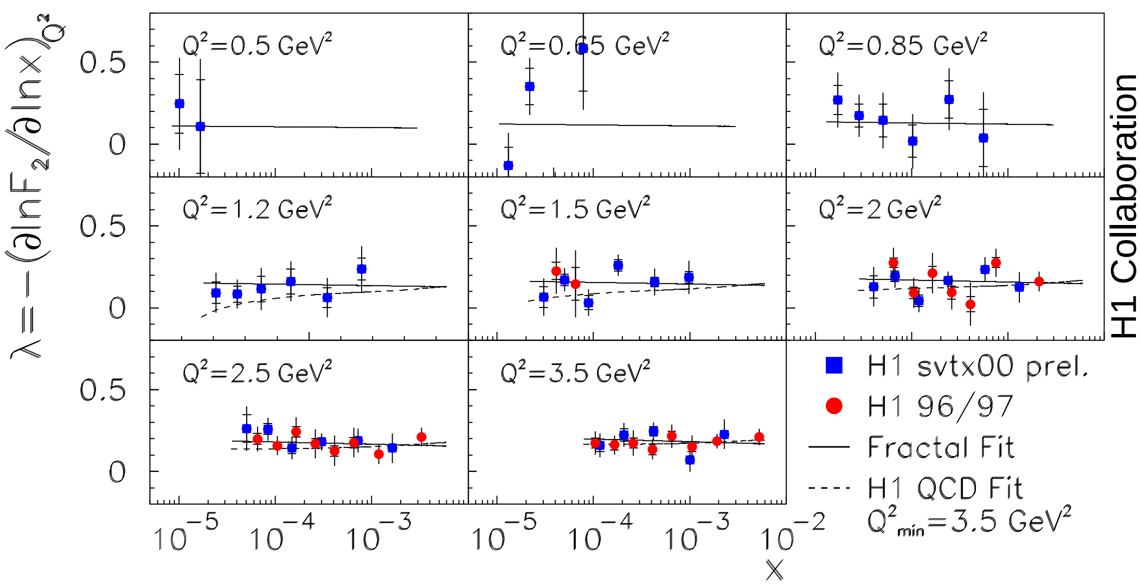

Figure 6: Measurement of the derivative function $\lambda(x, Q^2)$ with the present shifted vertex data (blue squares) and the nominal vertex data [19] (red points): the inner error bars represent the statistical uncertainty; the full error bars include the systematic uncertainty added in quadrature; the solid curves represent the fractal fit to the ZEUS BPT and published H1 data [4]; the dashed curves represent the extrapolation of the H1 NLO QCD fit [4] below the minimum Q^2 of 3.5 GeV^2.

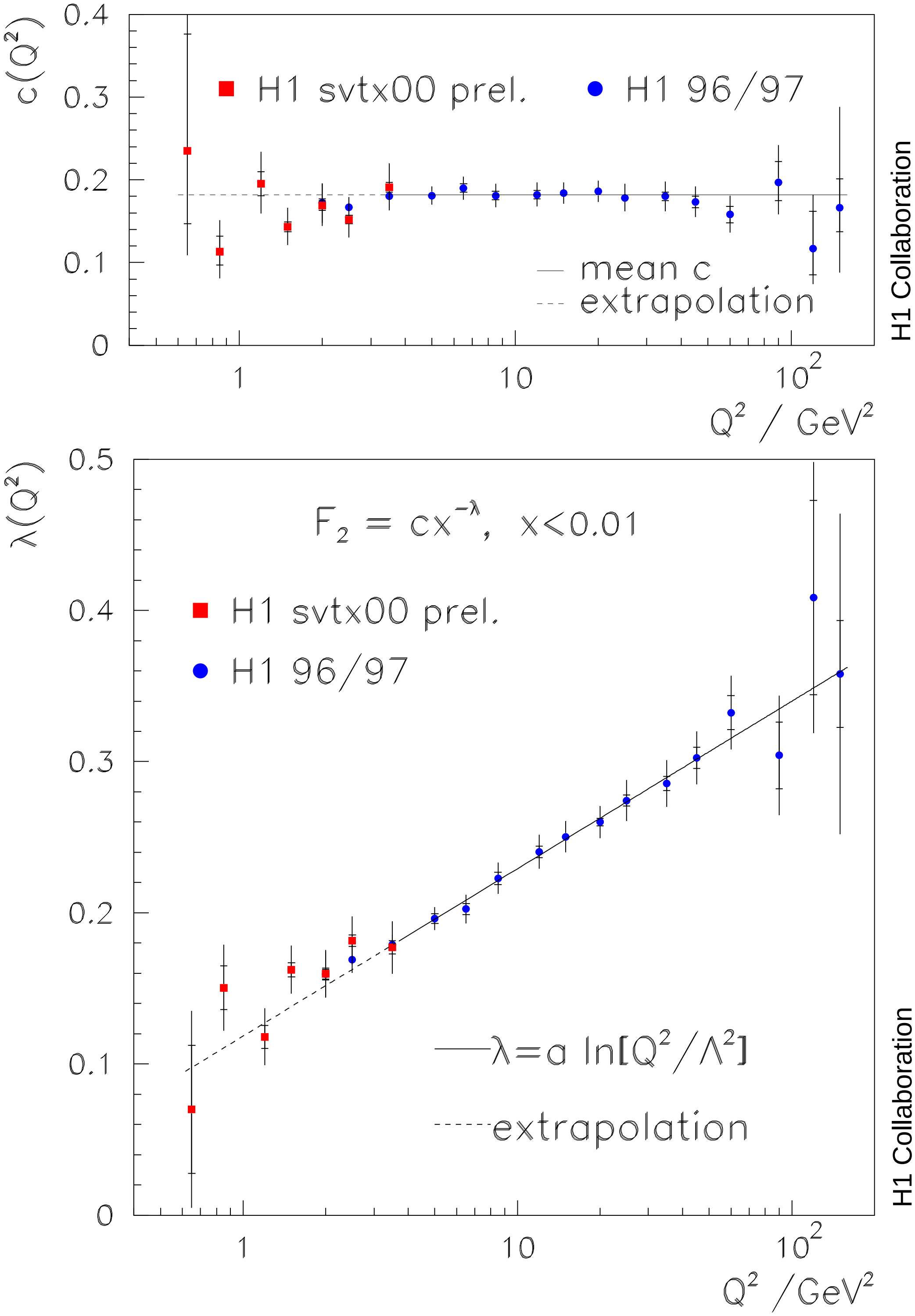

Figure 7: Determination of the coefficients $c(Q^2)$ (upper plot) and of the exponents $\lambda(Q^2)$(lower plot) from fits of the form $F_2(x, Q^2) = c(Q^2)x^{-\lambda(Q^2)}$: blue points - previous H1 structure function data [4] for $x \leq 0.01$; red squares - present data. The inner error bars illustrate the statistical uncertainties, the full error bars represent the statistical and systematic uncertainties added in quadrature. The straight lines represent the mean coefficient c (upper plot) and a fit of the form $a\ln[Q^2/\Lambda^2]$ (lower plot), respectively, using data for $Q^2 \geq 3.5$ GeV^2.

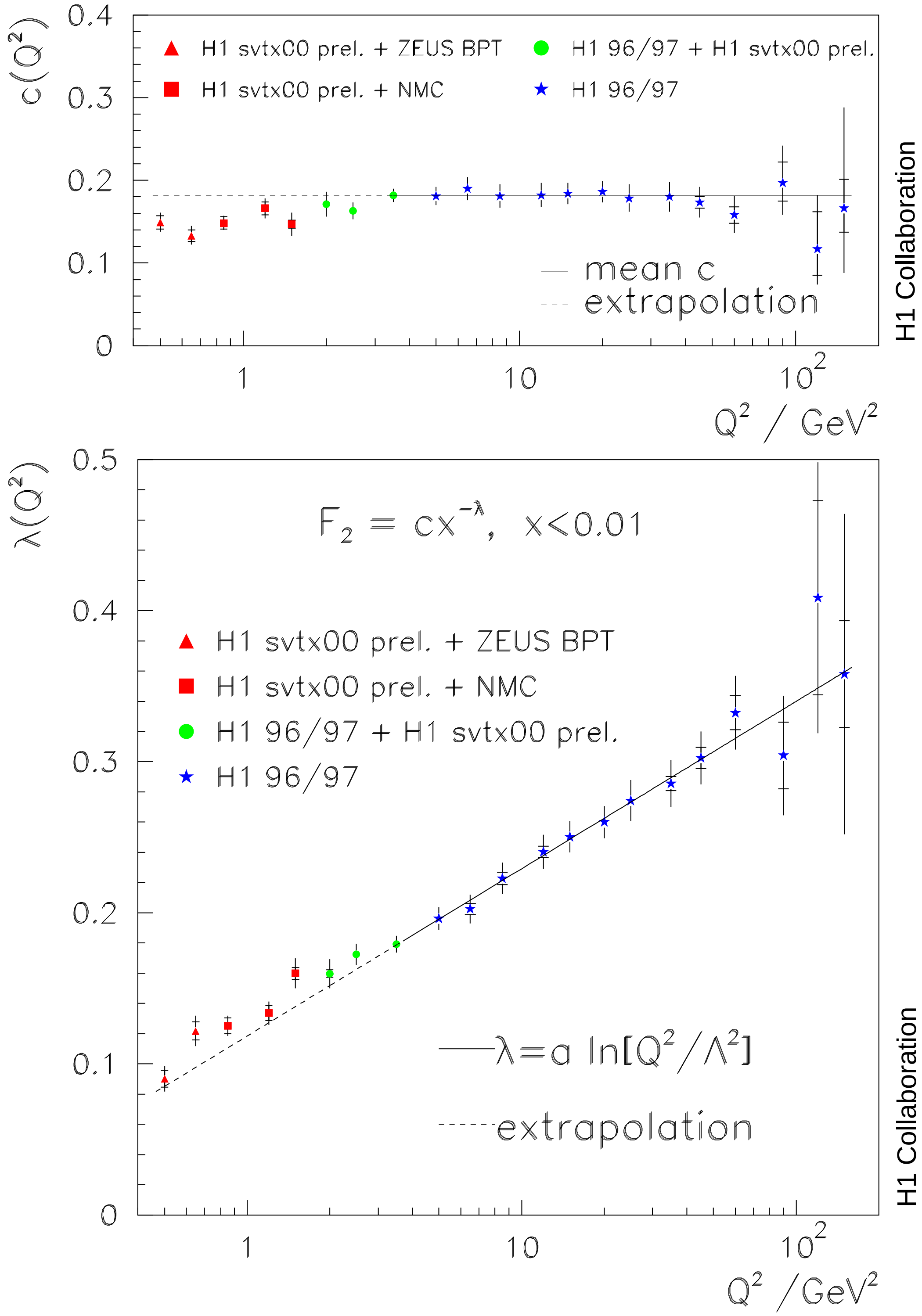

Figure 8: Determination of the coefficients $c(Q^2)$ (upper plot) and of the exponents $\lambda(Q^2)$(lower plot) from fits of the form $F_2(x, Q^2) = c(Q^2)x^{-\lambda(Q^2)}$ for $x \leq 0.01$: blue stars - previous H1 F_2 data [4]; green points - present data combined with the H1 data [4]; red squares - present data combined with NMC data; red triangles - present data combined with low Q^2 ZEUS BPT data [11]. The inner error bars illustrate the statistical uncertainties, the full error bars represent the statistical and systematic uncertainties added in quadrature. The straight lines represent the mean coefficient c (upper plot) and a fit of the form $a \ln[Q^2/\Lambda^2]$ (lower plot), respectively, using data for $Q^2 \geq 3.5$ GeV^2.